

Article

Lithium Plating Detection Based on Electrochemical Impedance and Internal Resistance Analyses

Yue Pan ¹ , Dongsheng Ren ^{1,2}, Xuebing Han ¹, Languang Lu ¹ and Minggao Ouyang ^{1,*}

¹ State Key Laboratory of Automotive Safety and Energy, Tsinghua University, Beijing 100084, China

² Institute of Nuclear and New Energy Technology, Tsinghua University, Beijing 100084, China

* Correspondence: ouymg@tsinghua.edu.cn

Abstract: Lithium plating, induced by fast charging and low-temperature charging, is one of the reasons for capacity fading and causes safety problems for lithium-ion batteries. Hence, reliable and effective non-destructive detection methods for lithium plating are needed. In this research, electrochemical impedance and internal resistance for batteries are measured during the rest period after charging. The results for lithium plating batteries and normal batteries are compared and analyzed. Lithium plating detection is realized with multiple indicators extracted from electrochemical impedance and internal resistance results. The effectiveness of the proposed detection methods is verified by the experiments conducted with commercial large-capacity batteries. The proposed methods have further potential to be used in battery management systems to realize online detection of lithium plating and improve the safety of battery systems.

Keywords: electrochemical impedance spectroscopy; lithium plating; lithium-ion battery; battery safety



Citation: Pan, Y.; Ren, D.; Han, X.; Lu, L.; Ouyang, M. Lithium Plating Detection Based on Electrochemical Impedance and Internal Resistance Analyses. *Batteries* **2022**, *8*, 206. <https://doi.org/10.3390/batteries8110206>

Academic Editors: Ottorino Veneri and Xuning Feng

Received: 1 September 2022

Accepted: 29 October 2022

Published: 2 November 2022

Publisher's Note: MDPI stays neutral with regard to jurisdictional claims in published maps and institutional affiliations.



Copyright: © 2022 by the authors. Licensee MDPI, Basel, Switzerland. This article is an open access article distributed under the terms and conditions of the Creative Commons Attribution (CC BY) license (<https://creativecommons.org/licenses/by/4.0/>).

1. Introduction

In the last decade, lithium-ion batteries have been widely used in energy storage systems [1], electric vehicles [2] and microgrid systems [3] due to their advantages of long cycle life, high energy density and high Coulombic efficiency. However, lithium-ion batteries still face capacity degradation and safety problems, leading to recalls or fire accidents of electric vehicles [4]. There are many reasons for battery capacity degradation and safety problems, among which lithium plating is a common cause [5].

In the case of lithium plating, the lithium-ions are deposited in metallic phase on the surface of graphite particles. Battery capacity degradation is caused by the reaction between the plated lithium metal and electrolytes. It is also proved that lithium plating can also cross the separator, inducing internal short circuit that may trigger thermal runaway [6]. Moreover, it is reported that the battery self-heating rate can be reduced to 110 °C due to severe lithium plating, which makes the battery prone to thermal runaway [7]. Therefore, it is important to detect lithium plating for both battery aging and battery safety considerations.

Janakiraman et al. [8] reviewed all the existing methods for lithium plating detection, categorizing the methods into the following 13 categories: (1) three-electrode diagnostics measuring the anode potential [9], (2) Coulombic efficiency measurement [10], (3) voltage relaxation and dV/dt calculation [11,12], (4) electrochemical impedance spectroscopy (EIS) measurement [13], (5) cell thickness measurement [14], (6) optical methods [15,16], (7) computed tomography measurement [17], (8) nuclear magnetic resonance spectroscopy [18], (9) neutron diffraction [19], (10) electron paramagnetic resonance spectroscopy [20], (11) acoustic method [21], (12) mass spectrometry titration [22], and (13) model-based anode potential observer [23,24].

From the above, most of the methods need additional tests with expensive equipment, which are not applicable to the battery management system (BMS) of electric vehicles and

energy storage stations. Only the voltage relaxation and the EIS measurement methods have further potential for online use. Many researchers have analyzed the voltage curve after lithium plating from different aspects, such as relaxation voltage [11], constant current discharging voltage [25] and dynamic discharging voltage [12]. However, only a few studies use electrochemical impedance and internal resistance behavior to detect lithium plating.

Electrochemical impedance spectroscopy is widely used to analyze the properties of electrochemical systems [26]. EIS can reflect the difficulty of the movement of charged particles, which is extensively used in battery modeling [27], battery temperature estimation, state of charge estimation, state of health estimation [28] and battery fault diagnosis [29,30]. In the area of lithium plating detection, Shinlder et al. [31] were the first to correlate lithium plating with EIS curves changes. Two main features were observed in EIS, including the shrinkage of the main semicircle representing the anodic charge transfer process and the decrease of high-frequency intersection resistance. Koleti et al. [32] studied the impedance during the battery charging process with periodic current interruptions. An anomaly impedance deviation indicating the onset of lithium plating is observed. Chen et al. [33] presented a method based on the distribution of relaxation times (DRT). The results show that lithium plating introduces a new charge transfer process on anode surface, leading to a decrease in peak intensity and a shift of peak position from normal range. Katzer et al. [34] revealed the relaxation impedance change process after lithium plating. Based on the root mean square error (RMSE) of an exponential fit function, a lithium plating detection method was proposed. Koseoglou et al. [35] utilized the dynamic EIS (DEIS) to continuously monitor the impedance during the charging process. When the semicircle exhibits an abrupt decrease, the onset of lithium plating can be detected. However, two important limitations arise in this research. Firstly, all the existing studies are conducted with batteries whose capacity is smaller than 4 Ah. It is not clear whether the impedance methods are applicable to large-capacity batteries. Secondly, it is still a great challenge to realize the reliable measurement of impedance in BMS. In contrast, the measurement of internal resistance is much easier to achieve. If lithium plating detection can be achieved only using internal resistance, the deployment cost of the detection method will be greatly reduced.

Therefore, the main novelty of this paper is analyzing the electrochemical impedance and internal resistance of large-capacity lithium-ion batteries with and without lithium plating and proposing indicators and detection methods based on the analyses. In Section 2, low-temperature charging experiments are conducted to induce lithium plating inside large-capacity commercial lithium-ion batteries. The lithium plating amount is quantified, and the electrochemical impedance and internal resistance are measured and analyzed. In Section 3, the electrochemical impedance and internal resistance results of batteries with and without lithium plating are analyzed. In Section 4, indicators are extracted from the electrochemical impedance and internal resistance results, and lithium plating detection methods are proposed. In Section 5, the conclusions of this study are summarized, and the outlook of the next-step research is proposed.

2. Experiment

In this study, commercial large-capacity pouch batteries with a nominal capacity of 24 Ah were tested. Detailed information can be found in Table 1. The battery capacity tests and low-temperature charging tests were conducted using a battery cycler (NEWARE CT8000). Battery temperature was controlled during the capacity tests and low-temperature tests using a thermostat chamber (GDBELL BE-TH-150M3). The EIS and internal resistance were tested using a commercial Autolab (Metrohm Autolab PGSTAT302N+BSTR 10A).

Table 1. Detailed information of the large-capacity batteries used in this study.

Property	Value
Producer	Wanxiang Group
Cathode material	$\text{Li}_x(\text{NiCoMn})_{1/3}\text{O}_2$
Anode material	Graphite
Cell type	Pouch
Charging cutoff voltage	4.2 V
Discharging cutoff voltage	2.5 V
Working temperature (Charging)	−25–55 °C
Working Temperature (Discharging)	−30–55 °C
Mass	0.5 kg
Length × Width × Thickness	225 × 160 × 7 mm

2.1. Capacity Test

Lithium plating causes capacity fading which can be measured by the capacity tests that were carried out before and after each low-temperature charging. The capacity tests were carried out at 25 °C, controlled by the thermostat chamber. Before each capacity test, the battery was placed inside the thermostat chamber for 3 h to ensure a consistent temperature inside and outside the battery. The capacity was then tested using 1/3C constant current (CC) and 4.2 V constant voltage (CV) charging until the current reached 1/20C, followed by a one-hour rest and 1/3C constant current discharging until the voltage reached 2.5 V. The charging and discharging were cycled 3 times, and the discharging capacity of the third cycle is taken as the result of the capacity test.

2.2. Low-Temperature Charging

In this study, low-temperature charging tests were conducted to induce lithium plating. All the charging tests were chosen to be conducted at −10 °C. Before each test, the tested battery, which was fully discharged in advance, was placed in the thermostat chamber at −10 °C for 3 h, followed by a CC-CV charging with different C-rates, as is listed in Table 2. Different C-rates were chosen to induce different amounts of lithium plating. After charging, there was a 10-h rest period, during which the electrochemical impedance and internal resistance were measured.

Table 2. Detailed setup of the experiments.

Group	No.	Charging C-Rate	Electrochemical Impedance or Internal Resistance
1	#1-1	0.10	Electrochemical impedance
	#1-2	0.33	Electrochemical impedance
	#1-3	0.50	Electrochemical impedance
	#1-4	1.00	Electrochemical impedance
2	#2-1	0.10	Internal resistance
	#2-2	0.20	Internal resistance
	#2-3	0.33	Internal resistance
	#2-4	0.50	Internal resistance

2.3. Electrochemical Impedance and Internal Resistance Measurement

Electrochemical impedance and internal resistance measurement were carried out during the rest period after charging. The electrochemical impedance was tested by the Autolab at potentiostatic mode, performing alternating current (AC) sine wave with 5 mV amplitude. In order to reduce the interference caused by voltage relaxation, electrochemical impedance under low frequency is untested. The selected frequency range is from 2 kHz to 0.1 Hz to shorten the test time and keep important information on the high and midfrequency regions. A total of 16 groups of impedance were tested during the voltage relaxation process at 0 min, 10 min, 20 min... 1 h, 2 h, 3 h... 10 h. The internal resistance was

tested by a ± 1 A pulse current (10 s 1 A charging–10 s rest–10 s 1 A discharging–10 s rest) continuously during the rest period. The 1s and 10s internal resistance can be calculated. Two groups of tests with batteries after different C-rate charging were carried out. Tests in Group 1 are electrochemical impedance tests, and Tests in Group 2 are internal resistance tests. The detailed settings of the tests are shown in Table 2.

The voltage profiles with electrochemical impedance and internal resistance measurement are shown in Figure 1. As is shown in Figure 1a, the voltage disturbance points are the electrochemical impedance test points. There are 16 test points in total during the rest period. In Figure 1b, the voltage profile is continuously disturbed by the pulse current, and the internal resistance can be calculated. Although disturbed by current, the voltage plateau caused by lithium plating can still be extracted from the original voltage profile. Therefore, the lithium plating detection method based on voltage plateau (dV/dt signal) [11] is also used for comparison.

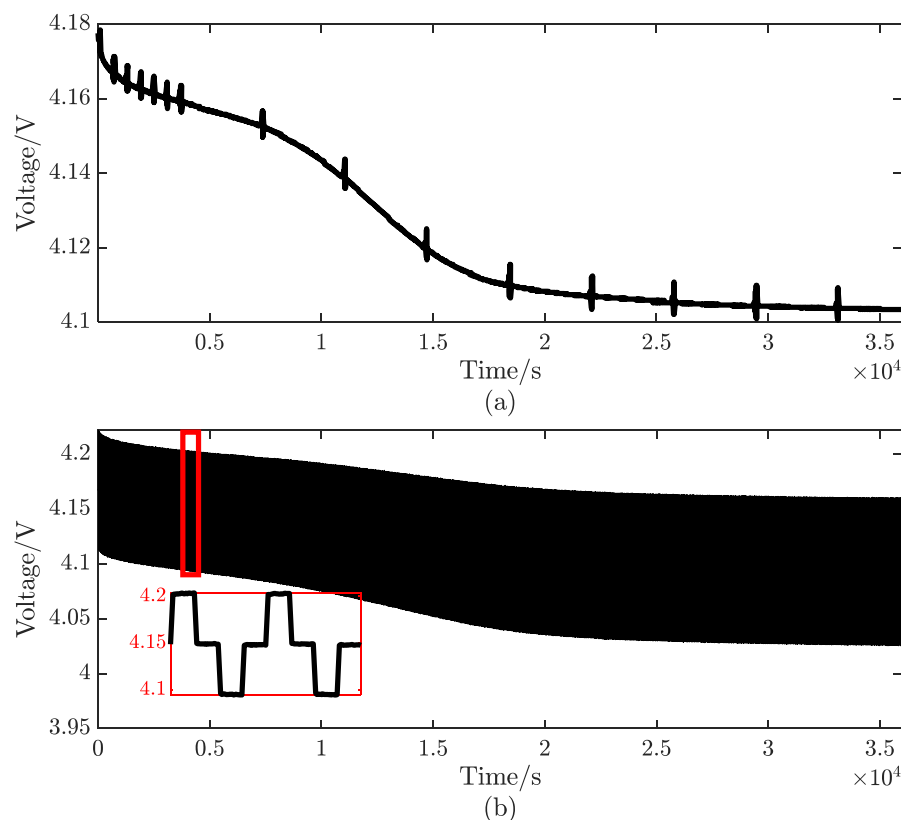


Figure 1. Voltage profiles with (a) electrochemical impedance and (b) internal resistance measurement.

3. Results and Analyses

3.1. Capacity Results

Capacity fading can be caused by many reasons, such as loss of lithium inventory and loss of active material of cathode and anode. In this study, the capacity fading is mainly caused by lithium plating since each low-temperature charging test only lasts ten hours or so. The capacity fading is described by the capacity change ratio, where a negative value indicates capacity fading, as is shown in Table 3.

Table 3. Capacity change ratio of low-temperature charging.

Group	No.	Capacity Change Ratio	Group	No.	Capacity Change Ratio
1	#1-1	+0.04%	2	#2-1	+0.04%
	#1-2	-2.18%		#2-2	-1.33%
	#1-3	-5.04%		#2-3	-3.31%
	#1-4	-7.30%		#2-4	-4.77%

The capacity change ratio of tests #1-1 and #2-1, whose charging C-rate is 0.1C, are close to zero. Therefore, no lithium plating happens in test #1-1 and test #2-1, and the electrochemical impedance and internal resistance of these tests can be regarded as the benchmark of no lithium plating (normal battery). Except for these two tests, the capacity change ratio of all the other tests is negative, indicating lithium plating happens in all the other tests. From tests #1-1 to #1-4, the absolute value of the capacity change ratio gets larger as the charging C-rate in Table 2 becomes larger. The same trend can also be found in tests #2-1~#2-4. As expected, there is a positive correlation between the amount of lithium plating and the charging C-rate.

3.2. Electrochemical Impedance Analyses

The electrochemical impedance results during the rest period after the charging of experiments group 1 (#1-1~#1-4) are shown in Figure 2. No diffusion behavior can be seen because of the narrow frequency range used in the experiments. The results colored in blue for each experiment are tested immediately after charging. The results colored in red are tested 10 h after charging. It is worth noting that the ranges of the *x*-axis and *y*-axis are different in Figure 2a-d since relative change during the rest period of each experiment is the focus in this section. The impedance results with the same coordinate range are shown in Figure A1a-d in Appendix A. As is shown in Figure 2a, the electrochemical impedance results of the normal battery (without lithium plating) only change slightly with time. Based on the capacity results, lithium plating happens in experiments #1-2, #1-3 and #1-4. As is shown in Figure 2b-d, the electrochemical impedance spectrum shrinks strongly at the beginning of the rest period for all the lithium plating batteries. Then the electrochemical impedance spectrum recovers gradually during the rest period, as is shown by the blue arrow in Figure 2. The recovery durations are different in different experiments, ranging from 3 h to 5 h. After 6 h, the electrochemical impedance spectrum hardly changes with time. However, unlike the results presented in Ref. [31] for small-capacity batteries, the electrochemical impedance of lithium plating batteries under high frequency changes differently with time in our study. The high-frequency impedance of experiments #1-3 and #1-4 gradually increase with time, as is marked by the red arrow in Figure 2, while that of experiment #1-2 is almost unchanged. Since the amount of lithium plating in experiments #1-3 and #1-4 is larger than that of experiment #1-2, it is assumed that the high-frequency impedance change may be correlated with the amount of lithium plating.

The DRT results are calculated with the free software DRTtools [36]. All the parameters are kept consistent in the calculation to ensure comparable DRT results. The settings of the DRT calculation are listed in Table 4, and the parameter definition can be found in Ref. [36].

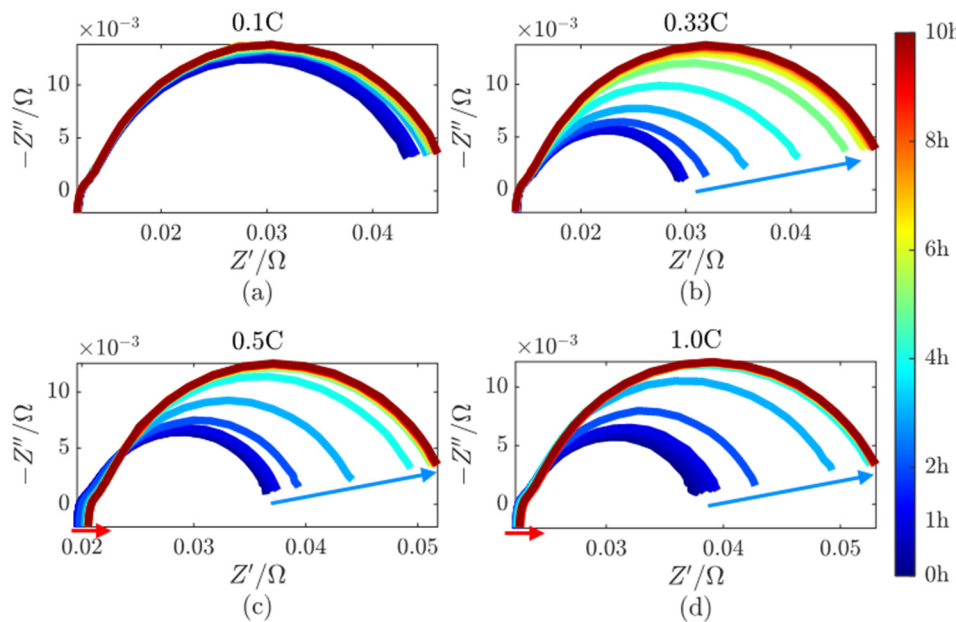


Figure 2. The electrochemical impedance spectrum of (a) experiment #1-1; (b) experiment #1-2; (c) experiment #1-3; (d) experiment #1-4.

Table 4. Detailed setup of DRT calculation.

Parameter	Setting
Method of discretization	Gaussian
Data used	Combined Re-Im Data
Inductance included	Fitting without inductance
Regularization derivative	1st-order
RBF shape control	FWHM Coefficient
Regularization parameter	2×10^{-3}

The DRT results of the electrochemical impedance spectrum are shown in Figure 3. Four peaks P1 (~500 Hz), P2 (~100 Hz), P3 (~8 Hz) and P4 (~0.3 Hz) are defined and marked. For a lithium-ion battery with NCM cathode and graphite anode, research has proven that when sorted from high frequency (small time constant) to low frequency (large time constant), the frequency of the contact process > the process of passive films (solid electrolyte interphase (SEI) and cathode electrolyte interphase (CEI)) > the charge transfer process [37–40]. Therefore, in this study, P1 (~500 Hz) could be correlated with the contact process. P2 (~100 Hz) could represent the process of the passive film, and P3 (~8 Hz) and P4 (~0.3 Hz) can be ascribed to the charge transfer process of the anode and cathode. When lithium plating happens, there is a right-shift and lower P3 and P4 and a missing P2 of the initial DRT result at the beginning of the rest period, indicating that the electrochemical process of SEI and charge transfer can be affected by lithium plating, as is shown by the blue curves in Figure 3b–d. During the rest period, P3 and P4 gradually shift to the left, with the peak intensity becoming increased and P2 gradually appearing. After 6 h, the DRT results of lithium plating batteries no longer change with time, and finally, the shape of the DRT profile is the same as that of a normal battery with 4 peaks that have similar peak height and frequency. Therefore, it is inferred that the shape change of the DRT profile after lithium plating is mainly caused by the lithium stripping process. Combined with the results presented in Ref [33], the plated reversible lithium may influence both the charge transfer process of the anode and the process of SEI passive film, leading to the decrease of peak intensity and shift of peak position. During the lithium stripping process, the DRT peaks gradually change. When the lithium stripping process ends, the DRT peaks recover back to normal.

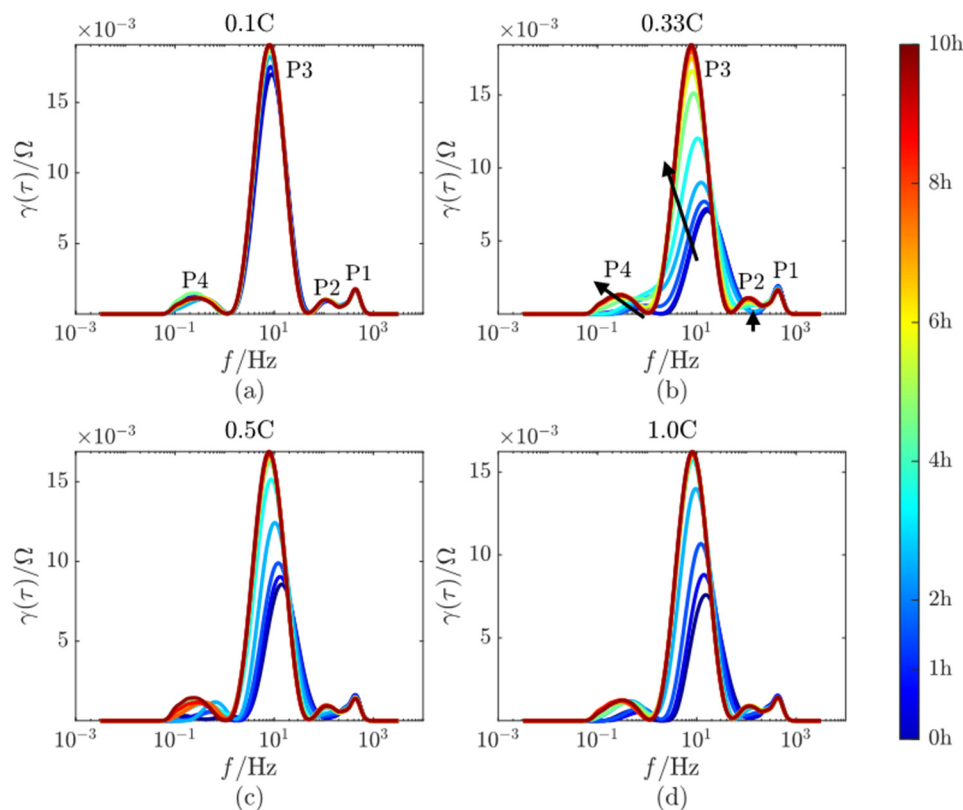


Figure 3. The DRT results of (a) experiment #1-1; (b) experiment #1-2; (c) experiment #1-3; (d) experiment #1-4.

To make the electrochemical impedance change clearer, the impedance values $|Z| = \sqrt{Z'^2 + Z''^2}$ under different frequencies are plotted versus time, as is shown in Figure 4. $\delta|Z|$ denotes the impedance change, as is defined in Equation (1):

$$\delta|Z|(t) = |Z|(t) - |Z|(0) \quad (1)$$

The maximum $\delta|Z|$ at 0.1 Hz is calculated and marked in each subfigure. For a normal battery, the impedance changes slightly with time, and the maximum $\delta|Z|$ at 0.1 Hz is 0.0029 Ω . For lithium plating batteries, there are significant impedance changes, especially at low frequencies, as is shown by the yellow curves in Figure 4b–d. The maximum $\delta|Z|$ at 0.1 Hz of lithium plating battery is an order of magnitude larger than that of a normal battery, which means that low-frequency impedance can be used as an indicator for lithium plating. However, the maximum $\delta|Z|$ at 0.1 Hz of lithium plating batteries does not increase with the amount of lithium plating, which means maximum $\delta|Z|$ at 0.1 Hz can only tell if lithium plating has occurred but cannot quantify the lithium plating amount.

3.3. Internal Resistance Analyses

The 1 s and 10 s internal resistance can be calculated during charging and discharging current pulse according to Equation (2):

$$\begin{cases} R_{t,\text{Cha}} = \left| \frac{V_t - V_0}{I_{\text{Cha}}} \right| \\ R_{t,\text{Dch}} = \left| \frac{V_t - V_0}{I_{\text{Dch}}} \right| \end{cases} \quad (2)$$

I_{Cha} is the charging pulse current (1 A) and I_{Dch} is the discharging pulse current (-1 A). V_0 is the voltage before charging and discharging the pulse. V_t is the voltage after t seconds of charging and discharging.

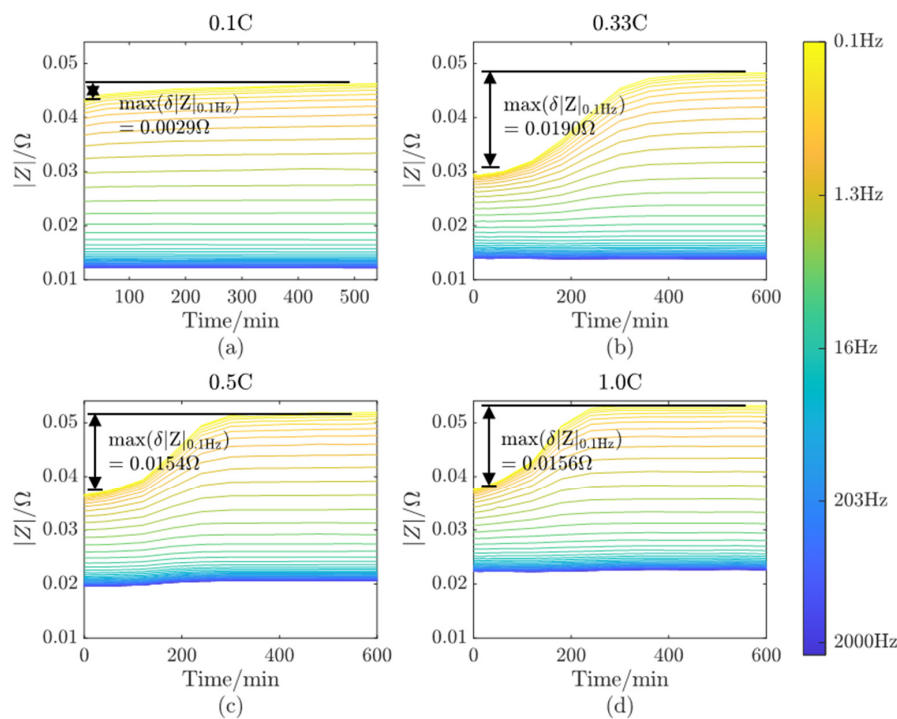


Figure 4. The impedance values at different frequencies of (a) experiment #1-1; (b) experiment #1-2; (c) experiment #1-3; (d) experiment #1-4.

The internal resistance results of experiment group 2 (#2-1~#2-4) are shown in Figure 5. The charging and discharging internal resistance nearly coincide with each other, while the 10 s internal resistance is slightly larger than the 1 s internal resistance for each experiment. The internal resistance curves of the same experiment have similar shapes. Basically, two major features can be summarized. Firstly, the internal resistance of all the experiments shows an increasing trend with different increasing patterns. For the battery without lithium plating, the internal resistance increases rapidly at the beginning (0–1 h) of rest and slowly thereafter, with an overall increase of 1 mΩ. For the lithium plating batteries, the internal resistance increases greatly in the first 5 h and then increases slightly in the next 5 h, with an overall increase of 2–3 mΩ, as is shown in Figure 5b–d. Secondly, the slope of the internal resistance curve of lithium plating batteries at the very beginning (0–1 h) of rest is smaller than that of normal battery, as is marked by the arrows in Figure 5. For experiments #2-3 and #2-4, the slope is even negative, which means the internal resistance decreases first at the very beginning of rest.

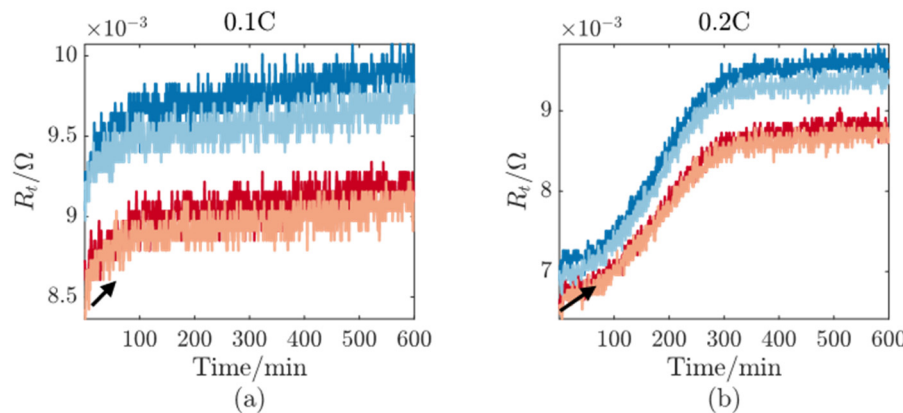


Figure 5. Cont.

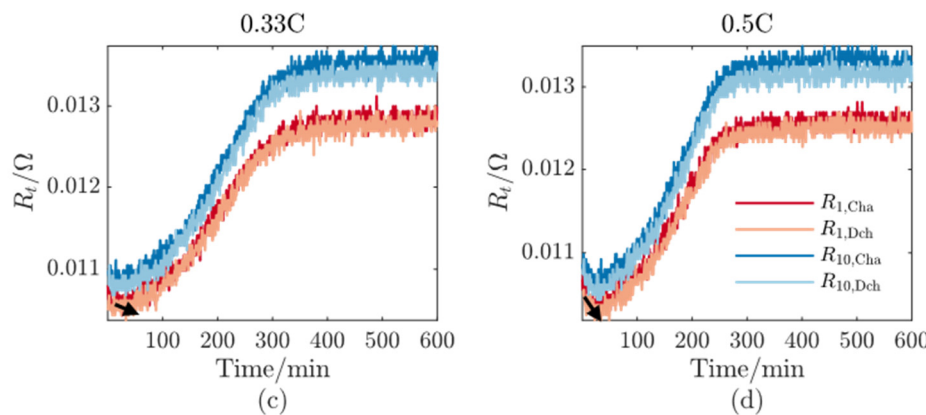


Figure 5. The internal resistance results of (a) experiment #2-1; (b) experiment #2-2; (c) experiment #2-3; (d) experiment #2-4.

4. Lithium Plating Detection Indicators and Methods

4.1. Lithium Plating Detection Based on Electrochemical Impedance

The electrochemical impedance change $\delta|Z|$ defined in Equation (1) is used as an indicator for lithium plating detection. The impedance changes $\delta|Z|$ under different frequencies from 0.1 Hz to 1 kHz are plotted in Figure 6. There is a significant difference in $\delta|Z|$ under 0.1 Hz and 1 Hz between the normal battery and all three lithium plating batteries, as is shown in Figure 6a,b. A threshold value, e.g., $\delta|Z| = 5 \times 10^{-3} \Omega$, can be set to realize the detection of lithium plating. For $\delta|Z|$ under frequencies no less than 10 Hz, the difference between normal batteries and lithium plating batteries is not that significant. $\delta|Z|$ for lithium plating battery in experiment #1-2 nearly coincides with that of normal battery, which means it is difficult to detect. Therefore, impedance under frequencies 1 Hz and 0.1 Hz are favored for lithium plating detection. With a preset threshold value, the impedance change $\delta|Z|$, which is larger than the threshold, indicates that the lithium plating has occurred in the charging process. However, this method can not quantify the amount of lithium plating.

4.2. Lithium Plating Detection Based on Internal Resistance

The 10 s charging internal resistance results $R_{10,\text{Dch}}$ for each experiment are used for lithium plating detection since the internal resistance curves of the same experiment have similar shapes. The internal resistance is filtered by first using the moving average method to remove the fluctuation caused by measurement noise. Then, the filtered internal resistance is normalized according to Equation (3):

$$R_{\text{Norm}} = \frac{R_{10,\text{Dch}}(t)}{R_{10,\text{Dch}}(0)} \quad (3)$$

Since the internal resistance is continuously tested during the whole 10-h resting period, the changing rate of internal resistance over time, denoted as dR/dt , can be calculated with the filtered results. The voltage differential (dV/dt) method [11] is a classical method for lithium plating detection. Therefore, the voltage signal is also analyzed here as a comparison with the internal resistance signal. The voltage signal is the superposition of relaxation voltage and the fluctuation caused by pulse current. To separate the relaxation voltage from the fluctuated voltage caused by pulse current, the variational mode decomposition algorithm, which is a non-recursive mode decomposition method proposed by Dragomiretskiy et al. [41], is used. Detailed information on the algorithm can be found in our previously published paper [12]. After the decomposition, dV/dt can be calculated with the relaxation voltage.

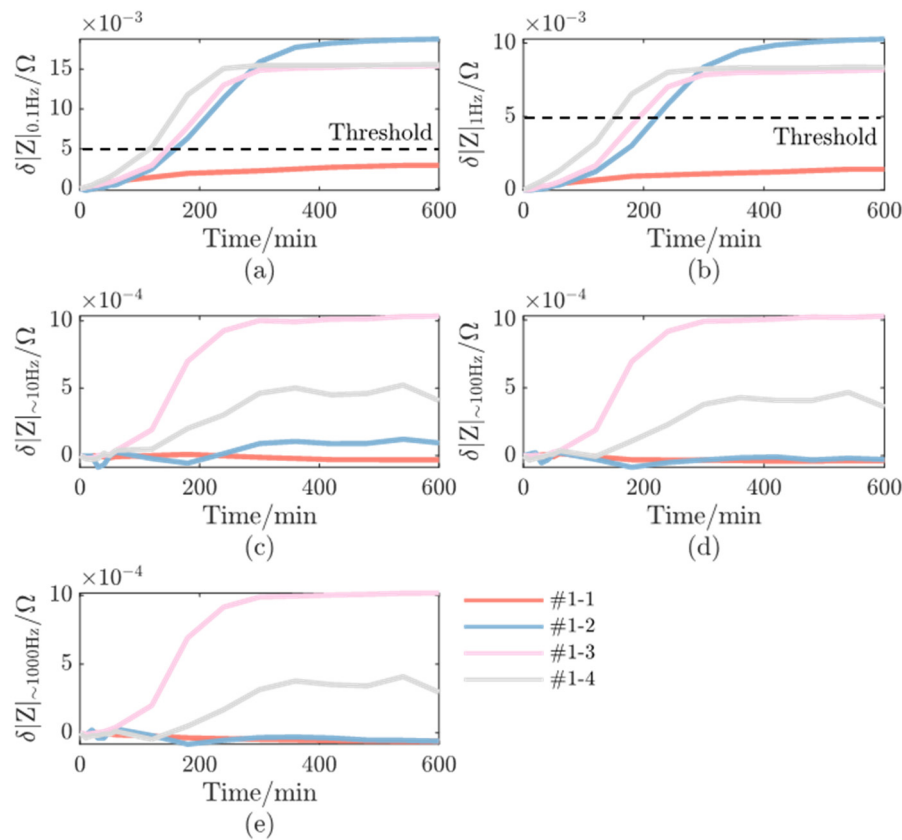


Figure 6. The electrochemical impedance changes $\delta|Z|$ of experiment group 1 at (a) 0.1 Hz; (b) 1 Hz; (c) around 10 Hz; (d) around 100 Hz; (e) around 1000 Hz.

The results are summarized in Figure 7. As is shown in Figure 7a,b, the filtered internal resistance curve and filtered voltage curve represents the shape of the original curve with removed fluctuations. The normalized internal resistance R_{Norm} of experiment group 2 are shown in Figure 7c and two features can be found. Firstly, the overall increase of R_{Norm} of lithium plating batteries is greater than that of normal battery, which is consistent with the analyses in Section 3.3. Therefore, a threshold can be set for lithium plating detection as is shown in Figure 7c. Compared with the lithium plating detection method based on voltage plateau, the internal resistance method with a preset threshold does not require a continuously measured internal resistance value. At a minimum, the internal resistance only needs to be measured twice, once at the beginning of relaxation and again after approximately 5 h. If the difference between these two measurements is larger than the threshold, there is lithium plating inside the battery. However, this method cannot quantify lithium plating. Secondly, R_{Norm} of lithium plating battery is smaller than that of normal battery at the beginning of tests, and the difference between them becomes larger as the amount of lithium plating increases, which is a possible indicator to distinguish the amount of lithium plating.

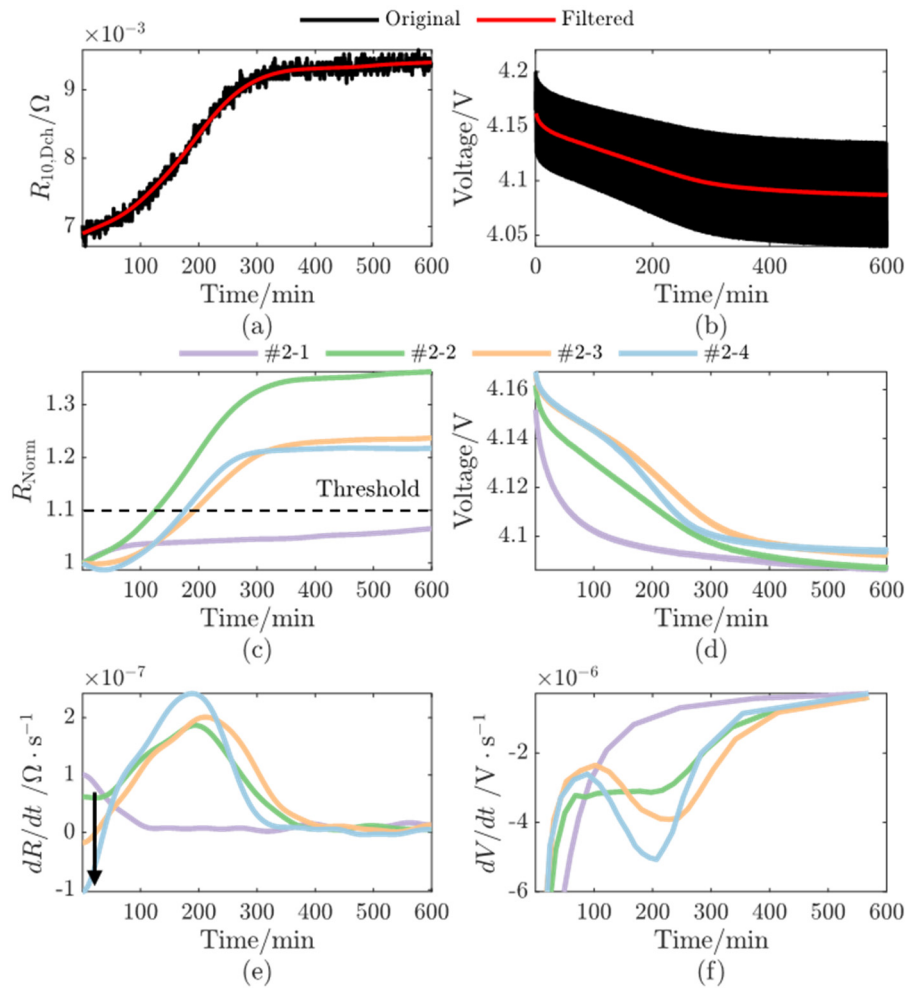


Figure 7. The internal resistance and voltage result. (a) Original and filtered internal resistance curve of experiment #2-2; (b) Original and filter voltage curve of experiment #2-2; (c) Normalized internal resistance R_{Norm} curves; (d) Relaxation voltage curves; (e) dR/dt curves; (f) dV/dt curves.

The dR/dt and dV/dt results are shown in Figure 7e,f. The lithium plating batteries each have a maximum peak in the dR/dt curves, corresponding with the minimum peak in the dV/dt curves. The time of the peaks in dR/dt curves also correspond well with those in dV/dt curves, which indicates that the peak of dR/dt curves could also be caused by the lithium stripping process. The dR/dt peak can be used as an indicator of lithium plating, but it is also not a quantitative indicator. Besides the dR/dt peak, more detailed information can be found in Figure 7e, marked by arrows. The dR/dt of lithium plating batteries is smaller than that of normal batteries at the beginning of the test, as is analyzed in Section 3.3, which is another candidate indicator to distinguish the amount of lithium plating.

The difference of R_{Norm} and dR/dt between normal battery and lithium plating battery is calculated, taking the value of normal battery #2-1 as a reference, as is defined in Equation (4):

$$\left\{ \begin{array}{l} \Delta R_{\text{Norm}} = R_{\text{Norm},i} - R_{\text{Norm},\text{ref}}, i = \#2-2 \sim \#2-4, \text{ref} = \#2-1 \\ \Delta dR/dt = dR/dt_i - dR/dt_{\text{ref}} \end{array} \right. \quad (4)$$

As is shown in Figure 8a,c. The minimum R_{Norm} difference and the minimum dR/dt difference are two indicators of lithium plating extracted from the curves. Figure 8b,d shows the two indicators versus the capacity change ratio. The capacity change ratio quantifies the amount of lithium plating, as is explained in Section 3.1. Therefore, the two

indicators that have a positive correlation with the capacity fading ratio can be used to distinguish the amount of lithium plating.

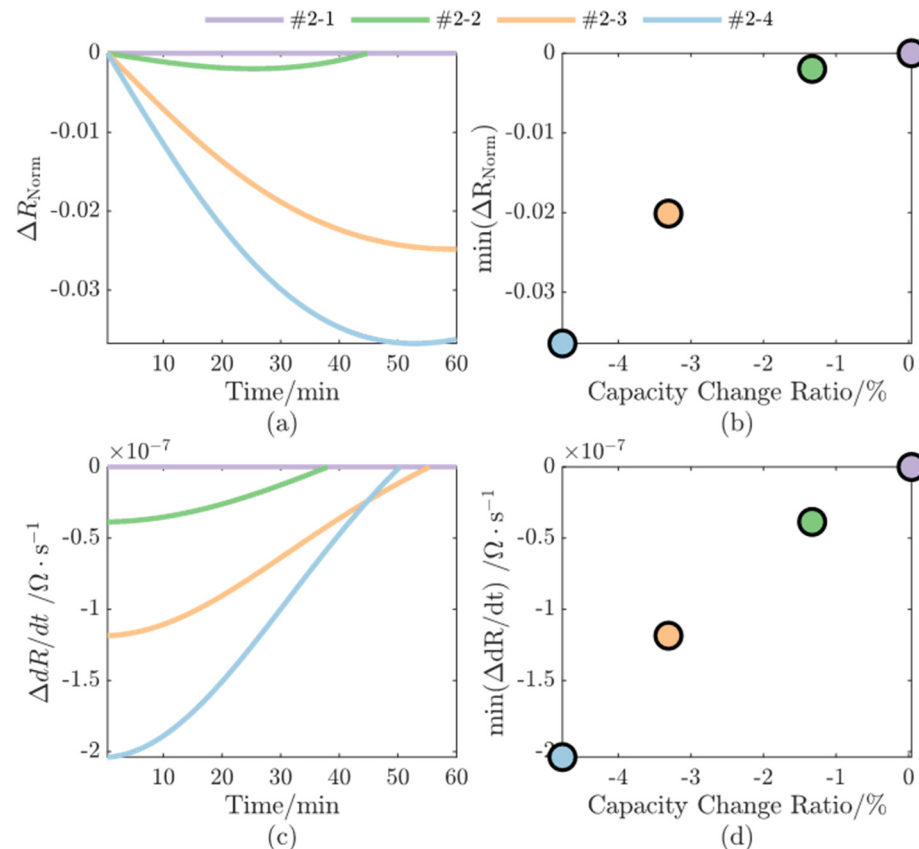


Figure 8. The difference of R_{Norm} and dR/dt between normal battery and lithium plating battery. (a) R_{Norm} difference; (b) The minimum of R_{Norm} difference versus capacity change ratio; (c) dR/dt difference; (d) The minimum of dR/dt difference versus capacity change ratio.

In summary, the internal resistance measured during the rest period after charging can be applied for lithium plating detection. Four indicators can be extracted from the internal resistance, namely the increase of R_{Norm} , the peak of dR/dt curve, the minimum R_{Norm} difference and the minimum dR/dt difference. The first two indicators have obvious distinctions between lithium plating batteries and normal batteries but cannot distinguish different amounts of lithium plating. The last two indicators can only be extracted at the beginning (in the first hour in this study) of rest but their relative magnitude can indicate the amount of lithium plating.

5. Conclusions

In this paper, we analyze the electrochemical impedance and internal resistance signal of lithium plating battery and normal battery during the rest period after charging. Indicators and detection methods for lithium plating are proposed and validated.

The electrochemical impedance results indicate that lithium plating causes the impedance spectrum to shrink strongly at the beginning of the rest period and then gradually return to normal. The corresponding DRT results indicate that the electrochemical process of SEI and charge transfer can be affected by lithium plating, causing peaks deviation and affecting peak intensity. The impedance value under low frequency (≤ 1 Hz) has significant variation during the rest period. Therefore, the impedance change under low frequency can be used as an indicator for lithium plating detection with a preset threshold value.

The internal resistance results of lithium plating batteries and normal batteries have different increase patterns, both in increase magnitude and slope. The extracted indicators

not only enable the detection of lithium plating but also can distinguish the amount of lithium plating. Compared with impedance measurement, the measurement of internal resistance is more applicable in nowadays BMS.

In our next-step research, the intrinsic inconsistency of impedance and internal resistance caused by battery aging and different temperatures will be taken into account to make the methods more practical.

Author Contributions: Conceptualization, Y.P.; methodology, Y.P.; software, Y.P.; validation, Y.P. and D.R.; formal analysis, D.R.; investigation, D.R.; resources, M.O.; data curation, Y.P.; writing—original draft preparation, Y.P.; writing—review and editing, Y.P.; visualization, Y.P.; supervision, L.L. and M.O.; project administration, L.L.; funding acquisition, D.R. and X.H. All authors have read and agreed to the published version of the manuscript.

Funding: This research was funded by National Natural Science Foundation of China, grant number No. 52007099, No. 52177217 and No. 52037006, and the Beijing Natural Science Foundation under the Grant No. 3212031.

Data Availability Statement: The data presented in this study are available on request from the corresponding author.

Conflicts of Interest: The authors declare no conflict of interest. The funders had no role in the design of the study; in the collection, analyses, or interpretation of data; in the writing of the manuscript; or in the decision to publish the results.

Appendix A

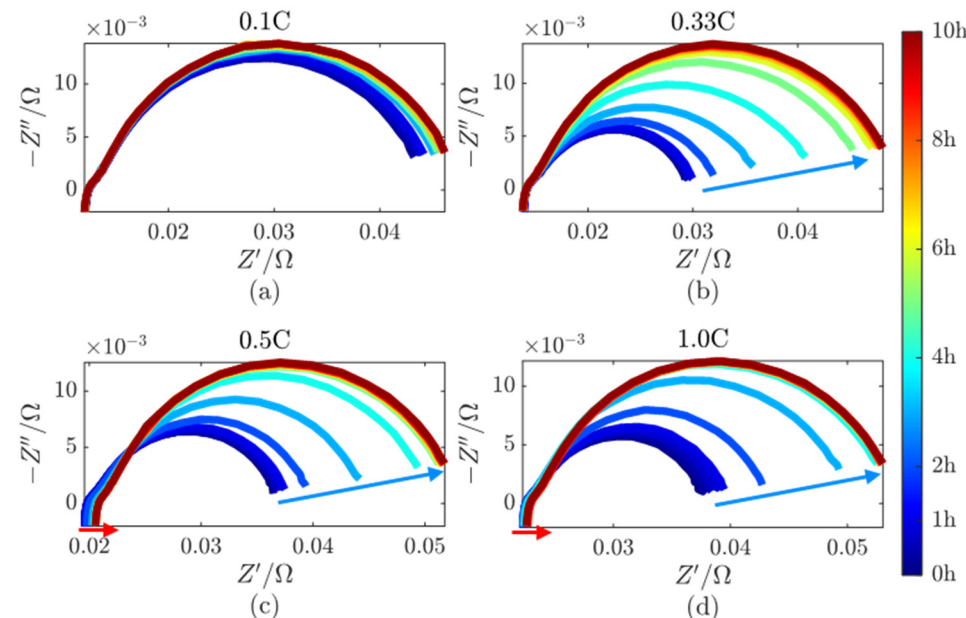


Figure A1. The electrochemical impedance spectrum of (a) experiment #1-1; (b) experiment #1-2; (c) experiment #1-3; (d) experiment #1-4.

A clear right shift can be seen when comparing the impedance results recorded at different C rates, which is caused by the degradation, specifically the internal resistance increase, of the battery after each low temperature test.

References

- Li, D.; Zouma, A.; Liao, J.T.; Yang, H.T. An Energy Management Strategy with Renewable Energy and Energy Storage System for a Large Electric Vehicle Charging Station. *eTransportation* **2020**, *6*, 100076. [[CrossRef](#)]
- Dixon, J.; Bell, K. Electric Vehicles: Battery Capacity, Charger Power, Access to Charging and the Impacts on Distribution Networks. *eTransportation* **2020**, *4*, 100059. [[CrossRef](#)]

3. Darcovich, K.; Recoskie, S.; Ribberink, H.; Michelet, C. The Impact of V2X Service under Local Climatic Conditions within Canada on EV Durability. *eTransportation* **2021**, *9*, 100124. [[CrossRef](#)]
4. Hu, G.; Huang, P.; Bai, Z.; Wang, Q.; Qi, K. Comprehensively Analysis the Failure Evolution and Safety Evaluation of Automotive Lithium Ion Battery. *eTransportation* **2021**, *10*, 100140. [[CrossRef](#)]
5. Liu, T.; Yang, X.G.; Ge, S.; Leng, Y.; Wang, C.Y. Ultrafast Charging of Energy-Dense Lithium-Ion Batteries for Urban Air Mobility. *eTransportation* **2021**, *7*, 100103. [[CrossRef](#)]
6. Klein, S.; Harte, P.; van Wickeren, S.; Borzutzki, K.; Röser, S.; Bärmann, P.; Nowak, S.; Winter, M.; Placke, T.; Kasnatscheew, J. Re-Evaluating Common Electrolyte Additives for High-Voltage Lithium Ion Batteries. *Cell Rep. Phys. Sci.* **2021**, *2*, 100521. [[CrossRef](#)]
7. Li, Y.; Feng, X.; Ren, D.; Ouyang, M.; Lu, L.; Han, X. Thermal Runaway Triggered by Plated Lithium on the Anode after Fast Charging. *ACS Appl. Mater. Interfaces* **2019**, *11*, 46839–46850. [[CrossRef](#)]
8. Janakiraman, U.; Garrick, T.R.; Fortier, M.E. Review—Lithium Plating Detection Methods in Li-Ion Batteries. *J. Electrochem. Soc.* **2020**, *167*, 160552. [[CrossRef](#)]
9. Lin, H.P.; Chua, D.; Salomon, M.; Shiao, H.C.; Hendrickson, M.; Plichta, E.; Slane, S. Low-Temperature Behavior of Li-Ion Cells. *Electrochem. Solid-State Lett.* **2001**, *4*, 71–74. [[CrossRef](#)]
10. Burns, J.C.; Stevens, D.A.; Dahn, J.R. In-Situ Detection of Lithium Plating Using High Precision Coulometry. *J. Electrochem. Soc.* **2015**, *162*, A959–A964. [[CrossRef](#)]
11. Ren, D.; Smith, K.; Guo, D.; Han, X.; Feng, X.; Lu, L.; Ouyang, M.; Li, J. Investigation of Lithium Plating-Stripping Process in Li-Ion Batteries at Low Temperature Using an Electrochemical Model. *J. Electrochem. Soc.* **2018**, *165*, A2167. [[CrossRef](#)]
12. Pan, Y.; Ren, D.; Kuang, K.; Feng, X.; Han, X.; Lu, L.; Ouyang, M. Novel Non-Destructive Detection Methods of Lithium Plating in Commercial Lithium-Ion Batteries under Dynamic Discharging Conditions. *J. Power Sources* **2022**, *524*, 231075. [[CrossRef](#)]
13. Wang, X.; Wei, X.; Zhu, J.; Dai, H.; Zheng, Y.; Xu, X.; Chen, Q. A Review of Modeling, Acquisition, and Application of Lithium-Ion Battery Impedance for Onboard Battery Management. *eTransportation* **2021**, *7*, 100093. [[CrossRef](#)]
14. Bitzer, B.; Gruhle, A. A New Method for Detecting Lithium Plating by Measuring the Cell Thickness. *J. Power Sources* **2014**, *262*, 297–302. [[CrossRef](#)]
15. Steiger, J.; Kramer, D.; Mönig, R. Microscopic Observations of the Formation, Growth and Shrinkage of Lithium Moss during Electrodeposition and Dissolution. *Electrochim. Acta* **2014**, *136*, 529–536. [[CrossRef](#)]
16. Sagane, F.; Shimokawa, R.; Sano, H.; Sakaebe, H.; Iriyama, Y. In-Situ Scanning Electron Microscopy Observations of Li Plating and Stripping Reactions at the Lithium Phosphorus Oxynitride Glass Electrolyte/Cu Interface. *J. Power Sources* **2013**, *225*, 245–250. [[CrossRef](#)]
17. Harry, K.J.; Hallinan, D.T.; Parkinson, D.Y.; MacDowell, A.A.; Balsara, N.P. Detection of Subsurface Structures underneath Dendrites Formed on Cycled Lithium Metal Electrodes. *Nat. Mater.* **2014**, *13*, 69–73. [[CrossRef](#)]
18. Arai, J.; Nakahigashi, R. Study of Li Metal Deposition in Lithium Ion Battery during Low-Temperature Cycle Using In Situ Solid-State ⁷Li Nuclear Magnetic Resonance. *J. Electrochem. Soc.* **2017**, *164*, A3403–A3409. [[CrossRef](#)]
19. Zinth, V.; Von Lüders, C.; Hofmann, M.; Hattendorff, J.; Buchberger, I.; Erhard, S.; Rebelo-Kornmeier, J.; Jossen, A.; Gilles, R. Lithium Plating in Lithium-Ion Batteries at Sub-Ambient Temperatures Investigated by in Situ Neutron Diffraction. *J. Power Sources* **2014**, *271*, 152–159. [[CrossRef](#)]
20. Wandt, J.; Jakes, P.; Granwehr, J.; Eichel, R.A.; Gasteiger, H.A. Quantitative and Time-Resolved Detection of Lithium Plating on Graphite Anodes in Lithium Ion Batteries. *Mater. Today* **2018**, *21*, 231–240. [[CrossRef](#)]
21. Bommier, C.; Chang, W.; Lu, Y.; Yeung, J.; Davies, G.; Mohr, R.; Williams, M.; Steingart, D. In Operando Acoustic Detection of Lithium Metal Plating in Commercial LiCoO₂/Graphite Pouch Cells. *Cell Rep. Phys. Sci.* **2020**, *1*, 100035. [[CrossRef](#)]
22. McShane, E.J.; McShane, E.J.; Colclasure, A.M.; Brown, D.E.; Brown, D.E.; Konz, Z.M.; Konz, Z.M.; Smith, K.; McCloskey, B.D.; McCloskey, B.D. Quantification of Inactive Lithium and Solid-Electrolyte Interphase Species on Graphite Electrodes after Fast Charging. *ACS Energy Lett.* **2020**, *5*, 2045–2051. [[CrossRef](#)]
23. Li, L.; Ren, Y.; O'Regan, K.; Koleti, U.R.; Kendrick, E.; Widanage, W.D.; Marco, J. Lithium-Ion Battery Cathode and Anode Potential Observer Based on Reduced-Order Electrochemical Single Particle Model. *J. Energy Storage* **2021**, *44*, 103324. [[CrossRef](#)]
24. Wu, L.; Pang, H.; Geng, Y.; Liu, X.; Liu, J.; Liu, K. Low-Complexity State of Charge and Anode Potential Prediction for Lithium-Ion Batteries Using a Simplified Electrochemical Model-Based Observer under Variable Load Condition. *Int. J. Energy Res.* **2022**, *46*, 11834–11848. [[CrossRef](#)]
25. Petzl, M.; Danzer, M.A. Nondestructive Detection, Characterization, and Quantification of Lithium Plating in Commercial Lithium-Ion Batteries. *J. Power Sources* **2014**, *254*, 80–87. [[CrossRef](#)]
26. Akkinenpally, B.; Reddy, I.N.; Manjunath, V.; Reddy, M.V.; Mishra, Y.K.; Ko, T.J.; Zaghib, K.; Shim, J. Temperature Effect and Kinetics, LiZr₂(PO₄)₃ and Li_{1.2}Al_{0.2}Zr_{1.8}(PO₄)₃ and Electrochemical Properties for Rechargeable Ion Batteries. *Int. J. Energy Res.* **2022**, *46*, 14116–14132. [[CrossRef](#)]
27. Zabara, M.A.; Katlrci, G.; Ülgüt, B. Operando Investigations of the Interfacial Electrochemical Kinetics of Metallic Lithium Anodes via Temperature-Dependent Electrochemical Impedance Spectroscopy. *J. Phys. Chem. C* **2022**, *126*, 10968–10976. [[CrossRef](#)]
28. Jiang, B.; Zhu, J.; Wang, X.; Wei, X.; Shang, W.; Dai, H. A Comparative Study of Different Features Extracted from Electrochemical Impedance Spectroscopy in State of Health Estimation for Lithium-Ion Batteries. *Appl. Energy* **2022**, *322*, 119502. [[CrossRef](#)]

29. Tanim, T.R.; Dufek, E.J.; Walker, L.K.; Ho, C.D.; Hendricks, C.E.; Christophersen, J.P. Advanced Diagnostics to Evaluate Heterogeneity in Lithium-Ion Battery Modules. *eTransportation* **2020**, *3*, 100045. [[CrossRef](#)]
30. Wildfeuer, L.; Lienkamp, M. Quantifiability of Inherent Cell-to-Cell Variations of Commercial Lithium-Ion Batteries. *eTransportation* **2021**, *9*, 100129. [[CrossRef](#)]
31. Schindler, S.; Bauer, M.; Petzl, M.; Danzer, M.A. Voltage Relaxation and Impedance Spectroscopy as In-Operando Methods for the Detection of Lithium Plating on Graphitic Anodes in Commercial Lithium-Ion Cells. *J. Power Sources* **2016**, *304*, 170–180. [[CrossRef](#)]
32. Koleti, U.R.; Dinh, T.Q.; Marco, J. A New On-Line Method for Lithium Plating Detection in Lithium-Ion Batteries. *J. Power Sources* **2020**, *451*, 227798. [[CrossRef](#)]
33. Chen, X.; Li, L.; Liu, M.; Huang, T.; Yu, A. Detection of Lithium Plating in Lithium-Ion Batteries by Distribution of Relaxation Times. *J. Power Sources* **2021**, *496*, 229867. [[CrossRef](#)]
34. Katzer, F.; Danzer, M.A. Analysis and Detection of Lithium Deposition after Fast Charging of Lithium-Ion Batteries by Investigating the Impedance Relaxation. *J. Power Sources* **2021**, *503*, 230009. [[CrossRef](#)]
35. Koseoglou, M.; Tsionumas, E.; Ferentinou, D.; Jabbour, N.; Papagiannis, D.; Mademlis, C. Lithium Plating Detection Using Dynamic Electrochemical Impedance Spectroscopy in Lithium-Ion Batteries. *J. Power Sources* **2021**, *512*, 230508. [[CrossRef](#)]
36. Wan, T.H.; Saccoccio, M.; Chen, C.; Ciucci, F. Influence of the Discretization Methods on the Distribution of Relaxation Times Deconvolution: Implementing Radial Basis Functions with DRTtools. *Electrochim. Acta* **2015**, *184*, 483–499. [[CrossRef](#)]
37. Illig, J.; Ender, M.; Weber, A.; Ivers-Tiffée, E. Modeling Graphite Anodes with Serial and Transmission Line Models. *J. Power Sources* **2015**, *282*, 335–347. [[CrossRef](#)]
38. Zhou, X.; Huang, J.; Pan, Z.; Ouyang, M. Impedance Characterization of Lithium-Ion Batteries Aging under High-Temperature Cycling: Importance of Electrolyte-Phase Diffusion. *J. Power Sources* **2019**, *426*, 216–222. [[CrossRef](#)]
39. Gantenbein, S.; Weiss, M.; Ivers-Tiffée, E. Impedance Based Time-Domain Modeling of Lithium-Ion Batteries: Part I. *J. Power Sources* **2018**, *379*, 317–327. [[CrossRef](#)]
40. Shafiei Sabet, P.; Stahl, G.; Sauer, D.U. Non-Invasive Investigation of Predominant Processes in the Impedance Spectra of High Energy Lithium-Ion Batteries with Nickel–Cobalt–Aluminum Cathodes. *J. Power Sources* **2020**, *472*, 228189. [[CrossRef](#)]
41. Dragomiretskiy, K.; Zosso, D. Variational Mode Decomposition. *IEEE Trans. Signal Process.* **2014**, *62*, 531–544. [[CrossRef](#)]